Earth and Planetary Science Letters 413 (2015) 70–78

Contents lists available at ScienceDirect

Earth and Planetary Science Letters

www.elsevier.com/locate/epsl

# A strategy for cross-calibrating U–Pb chronology and astrochronology of sedimentary sequences: An example from the Green River Formation, Wyoming, USA

Malka L. Machlus [a,*], Jahandar Ramezani [b], Samuel A. Bowring [b], Sidney R. Hemming [a], Kaori Tsukui [a], William C. Clyde [c]

[a] Lamont-Doherty Earth Observatory, Columbia University, Palisades, NY 10964, USA
[b] Earth, Atmospheric and Planetary Sciences, Massachusetts Institute of Technology, Cambridge, MA 02139, USA
[c] Earth Sciences, University of New Hampshire, Durham, NH 03824, USA

ARTICLE INFO

*Article history:*
Received 25 January 2014
Received in revised form 13 August 2014
Accepted 4 December 2014
Available online 15 January 2015
Editor: G.M. Henderson

*Keywords:*
cyclostratigraphy
astrochronology
U–Pb
zircon
Green River Basin
Eocene

ABSTRACT

Astronomical calibration of the geological timescale has been limited until recently by the precision and accuracy of radioisotopic dates, especially for pre-Neogene records. Uncertainties for radioisotopic dates of older strata were typically much larger than a single precessional cycle, and dates were often sparse, leading to the practice of orbital tuning of cyclic strata in order to astronomically calibrate the desired interval. Ideally, in order to test the assumptions of astronomical calibration with geochronology, it is necessary that the precision of radioisotopic dates be comparable to the period of the cycle being tested. The new U–Pb CA-TIMS (chemical abrasion–thermal ionization mass spectrometry) zircon dates reported here conform to this precision requirement, with $2\sigma$ analytical uncertainties from $\pm 11\,000$ to $\pm 52\,000$ years for seven volcanic ashes from the Wilkins Peak Member of the Green River Formation. The zircon dates have simple distributions with few outliers and allow accurate estimations of the eruption ages with potential inaccuracies of less than precessional cycle.

The Eocene Green River Formation (Wyoming, USA) has long been recognized as a record of cyclicly-deposited lacustrine sediments, and the abundant intercalated volcanic ashes make it a suitable place to test new approaches to astronomical calibration of cyclic strata. The abundance of different types of marker beds, including tuffs that are intercalated with the sedimentary cycles, guarantee an unambiguous correlation between sampling locations of dated tuffs on the margins of the basin and the basin center where the cyclicity is best developed, thus reducing any stratigraphic uncertainties to a fraction of (hypothesized) precession cycle.

Tuning-based orbital age models, accepted by the previous geochronology, significantly deviate from the new geochronology, whereas a previously rejected model that assumes a short eccentricity period of 125 ky is now allowed. In order to test possible explanations for the apparent 125 ky period, such as changes in orbital periods, or gaps in the sedimentary record, we present an iterative strategy to select future ashes for dating such that the astronomical calibration/testing is optimized. We iteratively contrast two ad-hoc age models that bracket the linear interpolation between the dated ashes. The optimal intervals for further dating are located where the deviations between the models exceed our reported uncertainties. We propose that the iterative approach described here should become the standard for establishing a rigorous orbital calibration of the stratigraphic record where sufficient ashes exist.



## 1. Introduction

Astronomically-paced signals embedded in strata can be used as precise chronometers and this recognition has led to a long-standing effort to calibrate the geologic timescale astronomically (see review in Hinnov, 2013). Presently, the geologic timescale (GTS2012, Gradstein et al., 2012) is calibrated by a full astronomical solution through the Oligocene. However, older parts of the timescale are calibrated with partial astronomical solutions applied to selected non-continuous (i.e., "floating") intervals (Hinnov and Hilgen, 2012). The main challenge in extending and improving the astronomically-calibrated timescale is to rigorously test the orbital origin of the sedimentary cycles and assign accurate and precise

* Corresponding author.
*E-mail address:* machlus@ldeo.columbia.edu (M.L. Machlus).

http://dx.doi.org/10.1016/j.epsl.2014.12.009
0012-821X/

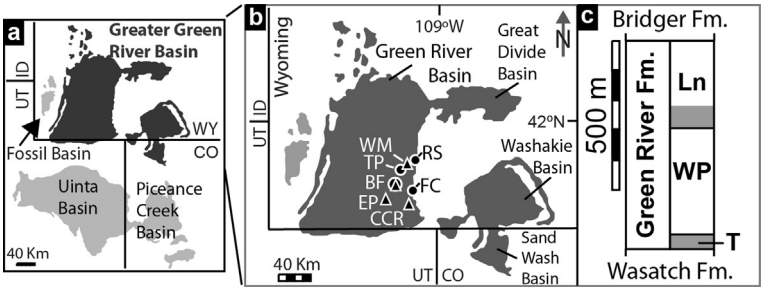


**Fig. 1.** Location map and general stratigraphy. (a) Extent (shaded) of the Green River Formation (Grande, 1984). (b) Location of cores (triangles), sampled tuffs (circles) and extent (dark shaded) of the Green River Formation in the Greater Green River Basin (Grande, 1984). Abbreviations of core names: WM, ERDA-LERC White Mountain 1; BF, ERDA-LERC Blacks Fork 1; EP, Union Pacific Rail Road Company El Paso 44-3; and CCR, U.S. DOE/LETC Currant Creek Ridge-1 (designated in the text as WM, BF, EP and CCR, respectively). Outcrop sampling locations: TP, Tollgate Rock (Main and Layered tuffs) and the Palisades (Sixth tuff); RS, Rock Springs (Grey tuff); FC, Firehole Canyon (Firehole and Second tuffs). Details of sampling locations are shown in Supplementary Material Table S1 and core locations are from Brownfield et al. (2011). (c) General stratigraphy for core BF near the center of the Green River Basin (Roehler, 1991a). Shaded intervals are composed mainly of organic rich micro-laminated carbonates, called oil shales; Members: T, Tipton; WP, Wilkins Peak; Ln, Laney.

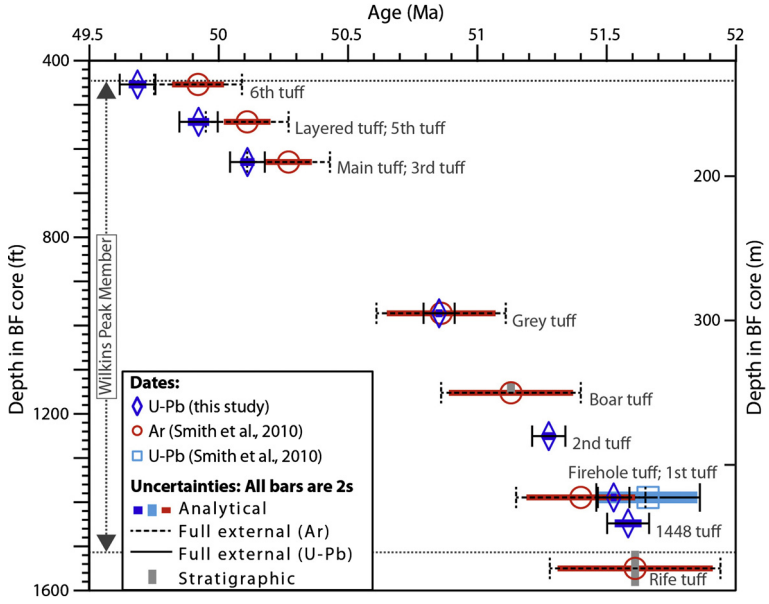


**Fig. 2.** Comparison between U–Pb and $^{40}Ar/^{39}Ar$ geochronology of tuffs in core BF. U–Pb dates reported here are weighted mean dates of individual zircon crystals (see Fig. 4, Table 1 and Supplementary Material Table S2). U–Pb and $^{40}Ar/^{39}Ar$ dates of Smith et al. (2010) are weighted mean dates of multi-crystal analyses, whereas two of their $^{40}Ar/^{39}Ar$ dates (Sixth and Rife tuffs) contain single crystal analyses in addition to multi-crystal analyses. $^{40}Ar/^{39}Ar$ ages are re-calibrated from Smith et al. (2003, 2008) using an age of 28.201 Ma (Kuiper et al., 2008) for the Fish Canyon sanidine standard (Smith et al., 2010). Stratigraphic uncertainties associated with the Rife tuff and the Boar tuff arise from uncertainties in correlating these tuffs from marginal sampling locations (Smith et al., 2003, 2008) to the location of core BF. All other ashes are identified in core BF (see Sections 2.3, 3.1, 4.1), but only one dated ash (1448 tuff) was actually sampled directly from core BF (see Supplementary Material Fig. S1 for in-core photo). Some tuffs have more than one name and the two most common names are listed here; the sources for the nomenclature are listed in Supplementary Material Table S1.

numerical ages to each cycle within the calibrated interval (Hinnov, 2013).

One of the limiting factors in achieving an astronomically-calibrated timescale has been the precision and accuracy of radioisotopic dates, especially for pre-Neogene records. Until recently, uncertainties of radioisotopic dates have been typically much larger than a single precessional cycle in pre-Neogene records, and dates are often sparse. This limitation has led to the practice of orbital tuning of apparently cyclic records in order to calibrate the desired interval (see review of tuning techniques in Hinnov, 2013). Orbital tuning involves the alignment of the record in question with an orbital target curve, and therefore can lead to circular reasoning. The ideal test would not include any a-priori assumptions about sediment accumulation rate.

Testing of hypothesized orbital forcing without a-priori assumptions can be achieved through two different avenues: statistically based tuning procedures and highly resolved and high-precision radioisotopic data. Newly developed quantitative statistical techniques include the 'average spectral misfit' method (Meyers and Sageman, 2007; Meyers, 2008; Meyers et al., 2012) and the Bayesian inverse method (Malinverno et al., 2010), and both methods address the timescale issues that caused circularity in past approaches to orbital tuning (see review in Hinnov, 2013). The resulting age-depth model from either method can be verified by the available, though typically sparse, radioisotopic data. Radioisotopic age control is the optimal means for direct testing, but it requires the availability of many datable ashes and it also requires that analytical uncertainties are comparable to or smaller than the precession period.

In this study, we use new radioisotopic data with analytical uncertainties comparable to the precession period (Figs. 1 and 2, Table 1), and demonstrate how such data can be used to test a hypothesized orbital pacing as well as to identify potential distortions that are introduced by variations in sediment accumulation rates. We use CA-TIMS (chemical abrasion-thermal ionization mass spectrometry) U–Pb dates on intercalated volcanic ashes (Table 1) to examine the apparent cyclicity of early Eocene lacustrine sediments of the Wilkins Peak Member of the Green River Formation

**Table 1**
Summary of calculated U–Pb ages and their uncertainties.

| Sample | Tuff | $\frac{^{206}Pb}{^{238}U}$ age | Uncertainty ($2\sigma$) | | | MSWD | $n$ |
|---|---|---|---|---|---|---|---|
| | | | $X$ | $Y$ | $Z$ | | |
| GR-416 | Sixth | 49.686 | 0.034 | 0.045 | 0.069 | 0.59 | 6 |
| WC07-10 | Layered | 49.919 | 0.040 | 0.051 | 0.074 | 0.72 | 8 |
| GR-411 | Main | 50.104 | 0.026 | 0.040 | 0.067 | 1.2 | 8 |
| GR-418 | Grey | 50.856 | 0.012 | 0.026 | 0.060 | 1.5 | 12 |
| GR-402 | Second | 51.279 | 0.020 | 0.033 | 0.064 | 1.1 | 9 |
| GR-401 | Firehole | 51.528 | 0.013 | 0.027 | 0.061 | 0.78 | 11 |
| GR-1448m | 1448 | 51.581 | 0.052 | 0.060 | 0.081 | 1.0 | 7 |

Note:
$X$: internal (analytical) uncertainty in the absence of all external or systematic errors.
$Y$: incorporates the U–Pb tracer calibration error.
$Z$: includes $X$ and $Y$, as well as the uranium decay constant errors.
MSWD: mean square of weighted deviates.
$n$: number of analyses included in the calculated weighted mean date.
Isotopic ratios utilized for age calculation are corrected for fractionation, spike, blank, and initial Th/U disequilibrium in magma (see Supplementary Material Table S2 for details of individual zircon analyses).

of Wyoming (Fig. 1). These sediments are unique, in that they contain so many zircon-bearing volcanic ashes, that if all were dated, a third of the precessional cycles (~30) of the resulting astrochronology would be directly dated. Such a comprehensive dating effort may not be practical, but nevertheless an accurate and detailed astrochronology for these particular strata has global importance in its own right as a means for improving the calibration of the early Eocene Geomagnetic Polarity Time Scale and for connecting the astrochronology established at the lake center to land-mammal evolution studied at the margin of these lacustrine deposits (e.g. Smith et al., 2010; Tsukui and Clyde, 2012).

Stratigraphic continuity of both marker beds and intercalated datable ashes is an additional requirement for reducing uncertainties in astrochronologic–radioisotopic intercalibration. In some cases like ours, the radioisotopic data are obtained from location(s) that may be in different basin(s) relative to location(s) where cyclostratigraphy is best developed (e.g. Kuiper et al., 2008). The calibrated astrochronology is then affected by the stratigraphic uncertainties of correlating several localities that are difficult to quantify. Our selected stratigraphic interval for this study contains abundant marker beds of different origins that are intercalated with datable ashes. Thus dated samples can be confidently correlated onto a specific part of a single precession cycle in the basin center, where the cyclostratigraphy is best developed. In other words, any radioisotopic date obtained from a marginal sample location can be correlated into the basin-center's cyclostratigraphy within the uncertainties associated with the sample date.

## 2. Geologic setting

### 2.1. The Green River Formation and suggested origins of cycles

The Green River Formation (Hayden, 1869) encompasses Eocene lacustrine strata deposited in several basins in Wyoming, Colorado and Utah (Bradley, 1929; Roehler, 1992a, 1992b; Fig. 1a) during the late stages of the Laramide orogeny (Dickinson et al., 1988; Prothero, 1996; Smith et al., 2008). In the Green River Basin of Wyoming (Fig. 1a), the continuous lacustrine interval of the Green River Formation is divided into the Tipton, Wilkins Peak and Laney members in ascending order (Fig. 1c). Sedimentary cycles of this formation in all the basins have long been attributed to orbital forcing (e.g., Bradley, 1929; Fischer and Roberts, 1991; Roehler, 1993; Bereskin and Morgan, 2001). Several orbital age models have been suggested based on radioisotopic ages (Smith et al., 2010 and references therein) particularly in the Wilkins Peak Member (Fig. 1c). Studies of the apparent cyclicity in the Wilkins Peak Member differ in their interpretations of significant cycles, how the depositional environments are affected by orbital pacing and whether sub-orbital cycles are significant (e.g., Pietras et al., 2003; Machlus et al., 2008; Meyers, 2008; Smith et al., 2010; Aswasereelert et al., 2013). Non-periodic origins have also been suggested and attributed to geomorphic controls on drainage stability and the sediment supply to paleo-lake Gosiute in which the Green River Formation was deposited (Pietras et al., 2003).

### 2.2. Sedimentary cycles of the Wilkins Peak Member

The Wilkins Peak Member (Fig. 1c) is characterized by laterally persistent, meter-scale sedimentary cycles that have been interpreted to be the result of lake fluctuations (Eugster and Hardie, 1975; Smoot, 1983; Roehler, 1993; Pietras et al., 2003; Pietras and Carroll, 2006). Each cycle typically has at its base organic-rich dolomitic mudstone, referred to as oil shale that is interpreted as the deeper lake condition. The oil shale is overlain by a sequence that is interpreted as transition to shallower lake (evaporite beds are present in some cycles) and followed by renewed deepening (see review in Machlus et al., 2008). The part of the cycle that is interpreted as the shallowest environment often shows evidence of sub-aerial exposure, and includes textures that are indicative of frequent wetting and drying of soil (Pietras and Carroll, 2006). Therefore, depositional hiatuses are likely to be frequent in the Wilkins Peak Member.

### 2.3. Laterally persistent marker beds and cycles of the Wilkins Peak Member

In order to confidently correlate cycles and dated ashes across a basin, it is necessary to identify laterally persistent stratigraphic units that are readily recognizable. There are several types of laterally continuous marker beds within the Wilkins Peak Member across the Green River Basin (see generalized columnar section in Culbertson et al., 1980). These markers include recognized oil shale beds that are part of the meter scale sedimentary cycles (Section 2.2; Culbertson et al., 1980; Roehler, 1991b), basin-wide clastic beds (units A through I of Culbertson, 1961), trona beds (Culbertson, 1966), radioactive zones (Love, 1964) and volcanic ashes (e.g., Culbertson et al., 1980; Smoot, 1983). Most markers are identifiable in both outcrops and cores. In this work we follow the nomenclature of Roehler (1991a, 1991b) for the oil shale beds, and Smith et al. (2003, 2008, 2010) for the tuffs that they studied, in order to facilitate the comparison of our results to previous geochronological studies.

## 3. Cyclostratigraphy

### 3.1. Basin wide cyclostratigraphies

Both Culbertson et al. (1980) and Roehler (1991b, 1993) defined basin-wide cycle-stratigraphies based on 77 meter-scale extensive oil shale beds as described in cores and outcrops in the Green River Basin. Each of the correlation schemes utilizes oil yield values as a proxy for oil shale beds and benefits from numerous down-hole records of oil yields (available online, see Brownfield et al., 2011). Although the resolution is not sufficient to examine sub-Milankovitch variability in detail (see review of in Machlus et al., 2008), the oil yields follow the sedimentary cycles, are correlated with total organic carbon, and provide adequate resolution for testing the orbital forcing hypothesis. Each of the 77 oil shale beds appears as a peak in an oil yield curve.

### 3.2. Decimeter scale cyclostratigraphies

Pietras and Carroll (2006) defined a decimeter-scale cycle-stratigraphy in a north-to-south transect of outcrops and cores from the eastern Green River Basin. This expanded cycle-stratigraphy builds on previous cyclostratigraphies (Section 3.1) and marker beds (see Section 2.3) and the refined cyclicity is interpreted as responses to lake level fluctuations (total of 126 decimeter to meter scale cycles in their most basinal studied location of core WM; Fig. 1b).

Aswasereelert et al. (2013) converted the stratigraphic sections and cores of Pietras and Carroll (2006) and Smith (2007) into a single north–south transect of 12 localities in the eastern Green River Basin. The facies assemblages they recognize are: alluvial, marginal lacustrine, and basinal lacustrine. The relative abundance of each facies association for all localities was calculated for each of the 52 time-equivalent surfaces they identified. Their approach provides a new numerical proxy for changes in lake depth that represents a wider range of lake depths compared with the previously used oil yields (Section 3.1), specifically, sedimentary cycles with overall low organic carbon that were excluded from the oil yield records (i.e. zero values) are represented in this approach.

## 4. Previous geochronology and orbital age models

### 4.1. Comparing age models in a single location

We chose core BF (Fig. 1b) as the optimal location for comparing all age models because it is the closest to the basin center and is also available for further inspection and sampling if necessary. Of the other four cores with available oil yield data for the entire member, core EP is not available for sampling and cores CCR and WM are more marginal than core BF (Fig. 1b).

All floating age models (Fig. 3), with the exception of the Meyers (2008) orbital model, were constructed in core BF; therefore no adjustments are needed for presenting them on an age-depth plot for this core. The age model of Meyers (2008) was re-scaled from core CCR to core BF. The anchored age models and our reported geochronology (Fig. 3) are based on ash samples that were not obtained in this particular core (except for the 1448 tuff), but the stratigraphic locations of our dated ashes in core BF (listed in Supplementary Material Table S1) are unambiguous because of the enclosing system of marker beds (e.g., Culbertson et al., 1980; Section 2.3). Each ash bed is referenced to bounding markers that are further constrained by additional markers. For example, oil shale beds that are integral to the sedimentary cyclicity (Section 2.2) are the immediate adjacent markers, whereas laterally continuous clastic beds, radioactive zones or trona beds are secondary supporting markers (Section 2.3). Each ash is identified relative to a specific part of a recognized oil shale bed and therefore

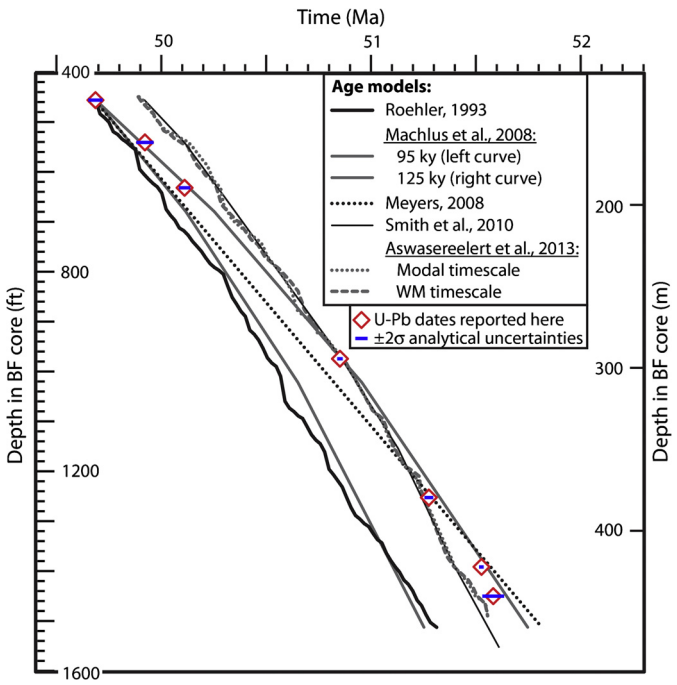


**Fig. 3.** Comparison between the U–Pb geochronology reported here and previous age models for core BF. Bars inside the diamonds are $2\sigma$ analytical uncertainties (column *X* in Table 1) associated with each date. Floating orbital age models are pinned to the youngest U–Pb date and include: Machlus et al. (2008) 125 ky and 95 ky eccentricity models; Meyers (2008) model for core CCR re-scaled for this core; and Roehler (1993) age model based on his definition of 77 precessional cycles. Fixed, non-floating age models include $^{40}Ar/^{39}Ar$ geochronology of Smith et al. (2010) (see also Fig. 2 for previous geochronology and uncertainties), and two anchored age models (modal timescale and WM timescale) of Aswasereelert et al. (2013) that are based on macro-stratigraphy and on Smith et al. (2010) ages.

is placed in a specific part of the precessional cycle. Thus the detailed stratigraphies (both Culbertson and Roehler, see Section 3.1) facilitate the exact correlation of each ash into a specific part of the precession cycle, even if the ash bed itself is within washed-out intervals of the core (depths of ashes in core BF and bounding oil shale beds are listed in Supplementary Material Table S1; see also Culbertson et al., 1980 for bounding marker beds). The stratigraphic uncertainty associated with correlating ashes may be a fraction of a precessional cycle if the orbital origin is accepted (see Section 2.3 and Supplementary Material Table S1).

### 4.2. Floating orbital age models

Floating orbital age models assume specific sediment accumulation rate(s) for the analyzed strata without assuming or relying on numerical ages. We show these models here as pinned to the U–Pb date for the Sixth tuff at the top of the Wilkins Peak Member (Fig. 3). There are four floating models: (1) Model based on the 77 numbered oil shale beds and associated sedimentary cycles of Roehler (1993; see Section 3.1) that were interpreted as precession cycles and assigned a mean period of 21 ky based on Laskar et al. (2004) solution for orbital parameters in the Eocene (Machlus et al., 2008); (2) Age model of constant sediment accumulation rate (Meyers, 2008) calculated from oil-yield values of core CCR (Fig. 1b) and re-scaled to core BF. The constant sedimentation rate corresponds to the minimal misfit between the spectrum of the age-modeled oil-yield curve and the expected orbital periods for this time period calculated by Berger et al. (1992) and Berger and Loutre (1991); (3) and (4) Two models derived from tuning an oil yield record to the interpreted short-eccentricity spectral peak, with periods of 95 ky and 125 ky, respectively (Machlus et al., 2008). Note that each of these models has a large uncertainty

envelope that is not shown for clarity (Fig. 3). When the uncertainty envelops associated with the age models (see Machlus et al., 2008; Section 4.3.2 and Fig. 4) are taken into account, neither model (or the intermediate 105 ky model) can be rejected with the geochronology of Smith et al. (2010; see also Section 4.4) given the relatively large uncertainties associated with those Ar ages.

### 4.3. Geochronology and age models

Smith et al. (2010) age model for the Wilkins Peak Member consists of six $^{40}Ar/^{39}Ar$ dates (Fig. 2) from the Sixth, Layered, Main, Grey, Boar and Firehole tuffs and two U–Pb dates from the Firehole tuff (Figs. 2, 3) and Analcite tuff in the overlying Laney Member. The U–Pb and $^{40}Ar/^{39}Ar$ dates of the same beds are indistinguishable when the $^{40}Ar/^{39}Ar$ dates of Smith et al. (2003, 2008) are recalculated to an age of 28.201 Ma (Kuiper et al., 2008) for the Fish Canyon sanidine standard. Smith et al. (2010) used the agreement between the two U–Pb dates and the $^{40}Ar/^{39}Ar$ dates to justify direct comparison between $^{40}Ar/^{39}Ar$-dated cycles of the Green River Formation and Laskar et al. (2004) astronomical solution for orbital eccentricity.

Three age models are anchored to Smith et al. (2010) $^{40}Ar/^{39}Ar$ geochronology (Fig. 3): (1) The age model of Smith et al. (2010) uses all $^{40}Ar/^{39}Ar$ dates and assumes constant sediment accumulation rate between any two dated ashes (thin black line in Fig. 3). Based on this model, the authors hypothesize that periods of fluvial deposition (fluvial beds within units A through I of Culbertson; Section 2.3) coincide with minima in long and short eccentricity as calculated by Laskar et al. (2004).

The other two age models (WM and modal age-models; dashed grey and dotted grey lines respectively, in Fig. 3; Aswasereelert et al., 2013) are based on decimeter scale macrostratigraphy (Section 3.2) and are anchored to the $^{40}Ar/^{39}Ar$ geochronology with varied sediment accumulation rates between any two dated ashes (the Sixth, Layered, Main, Grey, Boar, and Firehole tuffs). Aswasereelert et al. (2013) identified a strong short-eccentricity signal in spectra of all facies associations, ranging from predominant lacustrine to predominant alluvial facies. This interpretation connects short-eccentricity cycles with the recurrence of alluvial environments, in contrast to previous interpretations linking these cycles to lake level fluctuations.

### 4.4. Previous testing of orbital age models

Floating orbital age models that were evaluated on or before 2008 (Machlus et al., 2008; Meyers, 2008) must now be re-evaluated because the $^{40}Ar/^{39}Ar$ geochronology of Smith et al. (2003, 2008) was re-calculated by Smith et al. (2010) to account for the updated age estimate of the Fish Canyon sanidine used as a standard neutron flux monitor in Ar/Ar chronometry. Kuiper et al. (2008) estimated a Fish Canyon sanidine standard age of $28.201 \pm 0.046$ ($2\sigma$) Ma, more than 0.5% older than the previously accepted value of $28.02 \pm 0.28$ ($1\sigma$) Ma (Renne et al., 1998). Although the "true" age of the Fish Canyon sanidine standard is still an active area of research, we do not review the effects of different estimates on tests of orbital age models because the precision of our new U–Pb geochronology is better suited to the goal of orbital testing than the available Ar data.

The previously rejected 125 ky age model (Machlus et al., 2008; Section 4.2) is now consistent with the Smith et al. (2010) recalibrated $^{40}Ar/^{39}Ar$ geochronology; whereas the previously accepted Meyers (2008) age model (rescaled from core CCR, see Section 4.2) is no longer consistent. All other floating age models are also consistent with Smith et al. (2010) $^{40}Ar/^{39}Ar$ ages when they are pinned to the youngest date (Sixth tuff, Figs. 2, 3). The two age

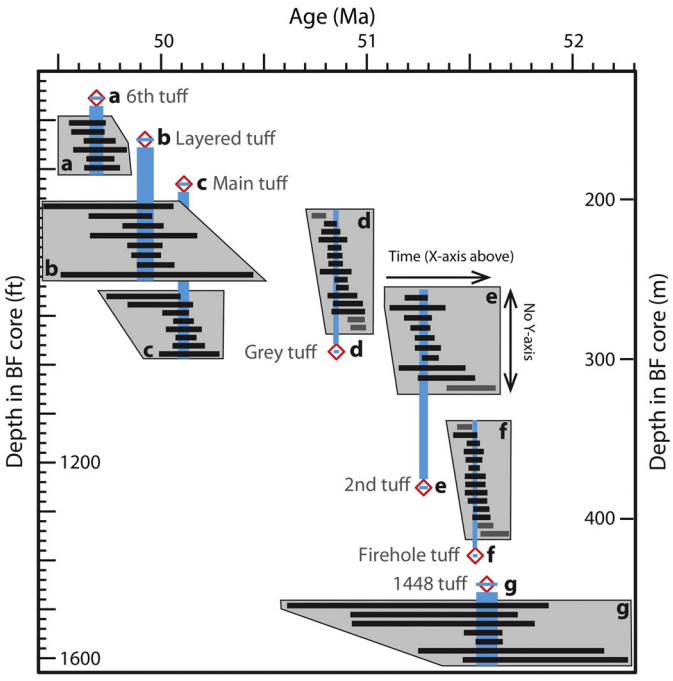


**Fig. 4.** Details of U–Pb geochronology. Weighted mean $^{206}Pb/^{238}U$ dates (diamonds, a–g) are plotted against depth of tuff beds in core BF. Each inset (a–g) displays individual zircon analyses (horizontal bars) with their $2\sigma$ analytical errors (bar widths) from a dated tuff. Vertical bars and their thicknesses (also bars inside diamonds) represent the weighted mean dates and their 95% confidence uncertainties with respect to the age axis. Solid black bars are analyses used in weighted mean calculation and grey bars are excluded (see Section 5.2.1 for explanation). The depth axis corresponds to the calculated weighted means (diamonds) only. See Supplementary materials for tabulated U–Pb data (Table S2), as well as analyses that plot outside this figure (Fig. S3).

models of Aswasereelert et al. (2013) are based on the geochronology of Smith et al. (2010) and are very close to each other and to the line connecting these dates (Fig. 3). In summary, most of the different astronomical age models reported in the literature for the Wilkins Peak Member cannot be rejected using Smith et al. (2010) $^{40}Ar/^{39}Ar$ geochronology due to $2\sigma$ analytical uncertainties of $\pm 90$ ky–240 ky for the six ashes within the Wilkins Peak Member (Fig. 2). A decrease of 5- to 10-fold in the uncertainties of radioisotopic dates is required to be able to test different age models.

## 5. U–Pb geochronology

### 5.1. Analytical methods

Zircons were separated from six outcrop samples (0.5–5 kg each), and one drill core split (sample GR-1448m, $<10$ g in weight; Supplementary Materials: Fig. S1). Sample locations and descriptions are provided in the Supplementary Materials (Table S1), and depths in core BF are shown in Fig. 2, Fig. 4 and in Table S1. For thick, internally graded, tuff layers (e.g., Main and Sixth tuffs), the lowermost part of each tuff was sampled. These basal parts contain abundant visible phenocrysts of biotite, and, in some tuffs, hornblende. Samples were processed by standard crushing and water-washing methods and heavy-mineral concentrates were obtained using magnetic separation and high-density liquids. Final zircon selection was carried out by hand picking and with the aid of a binocular microscope.

For analysis, we preferentially selected prismatic or acicular zircons with axial melt (glass) inclusions and without rounded edges or frosting. All analyses were performed on single zircon grains, pre-treated with a chemical abrasion (CA-TIMS) tech-

nique modified after Mattinson (2005), and spiked with a mixed $^{205}Pb$–$^{233}U$–$^{235}U$ (EARTHTIME ET535) tracer solution. Details of analytical procedures, weighted mean date calculation and error reporting are identical to those described in Ramezani et al. (2011). For reduction of raw data, propagation of uncertainties and date calculation, computer applications Tripoli and U–Pb Redux were used (Bowring et al., 2011; McLean et al., 2011). Complete U–Pb analytical data are listed in the Supplementary Materials (Table S2).

### 5.2. Results and interpretation

#### 5.2.1. Weighted mean dates and tuff ages

Weighted mean $^{206}Pb/^{238}U$ dates are calculated for each tuff sample based on the statistically coherent cluster of the youngest zircon analyses, after excluding analyses interpreted as outliers (see below), and are interpreted as reliable estimates of the eruption age (Table 1 and Fig. 4). This is done on a case-by-case basis that is described in detail in the Supplementary Materials (Section S5.2). Given a sufficient number of zircon analyses for each rock, identification of outliers out of a dominant population can be done objectively. In this study, from 80% to 100% of analyses from each sample have been used in the weighted mean date calculation, after excluding obviously xenocrystic zircons (i.e., pre-Eocene, Table S2 and Fig. S3 in Supplementary Material). In two instances (Grey Tuff, Firehole Tuff) the youngest single zircon has been excluded as an outlier (see explanation below). Detailed date distribution plots and Concordia diagrams accompanied by a discussion on each sample and how the weighted mean was calculated are presented in Supplementary Materials (Section S5.2 and Fig. S2, S3).

A suite of high-precision weighted mean dates from successive tuff beds that are mutually exclusive outside uncertainties and unequivocally obey stratigraphic order can serve as robust constraints on the ages of sediment deposition (e.g., Ramezani et al., 2011; Burgess et al., 2014). We interpret tuff beds of this study as primary deposits that settled through the water column in deep water, without any field or petrographic evidence for re-suspension and deposition by currents or slumping. All but one of the calculated weighted mean dates are statistically distinguishable outside their $2\sigma$ analytical uncertainties (from 11 ky to 40 ky) and none violate stratigraphic superposition. The weighted mean date of the 1448 tuff appears to overlap within $2\sigma$ uncertainty with that of the Firehole tuff above, only because the former had a distinctly higher uncertainty (52 ky) due to the small size of its zircons (low measured radiogenic Pb) that were extracted from a small-size core sample (Fig. S1 in Supplementary Material).

#### 5.2.2. Assessing the accuracy of age results

*5.2.2.1. Evaluation of populations* The assumption behind a geologically meaningful weighted mean date is the expectation of a single age population with normally distributed uncertainties. The accuracy of U–Pb dates thus depends on the extent to which the effects of geologically-driven, open system behavior among zircons can be mitigated. Subtle open system behavior is often difficult to detect and stems from either the potential for the presence of slightly older (pre-eruption age) zircons in the tuff or the potential for some zircons to produce younger dates relative to the eruption age because of lead-loss (Bowring et al., 2006).

In the tuff samples of this study careful zircon selection based on grain morphology has been highly successful in screening out old xenocrystic grains. An apparent exception has been the 1448 tuff core sample in which the paucity of available zircon due to small sample volume highly limited our grain selection. In addition, zircon pre-treatment by chemical abrasion has been highly effective in eliminating zircon domains affected by radiation-induced Pb loss. Nevertheless, residual Pb loss resulting in significantly younger dates (e.g., Grey tuff analysis z4; youngest zircon in Fig. 4d) may occasionally occur. For this reason, the youngest single zircon cannot always serve as the best estimate for the age of a sample. It can be demonstrated that inclusion of outliers suspected of subtle open system behavior in weighted mean calculations does not change the main conclusions of this study (see Supplementary Materials, Section S5.2).

There are a number of studies on complex silicic eruptions that have demonstrated very complex distributions of zircon dates related to complex magma chamber dynamics and incorporation of slightly older volcanic debris in the eruption (e.g., Rivera et al., 2013; Wotzlaw et al., 2013, 2014). However, modern high-precision U–Pb geochronologic studies have shown that many eruptive units are not that complex (Crowley et al., 2007; Burgess et al., 2014), and even in very complex magmatic systems (e.g., Rivera et al., 2013; Wotzlaw et al., 2013, 2014) it is possible to identify the youngest age population that formed shortly prior to eruption. Overall, our ability to detect and account for complexities in U–Pb systematics of volcanic zircons is a direct function of the precision of U–Pb analyses, as well as the quantity of data required to objectively identify statistical outliers.

*5.2.2.2. Initial Th–U disequilibrium in magma* Zircon $^{206}Pb/^{238}U$ dates must be corrected for initial $^{230}Th$ disequilibrium in magma, which results in a deficiency of $^{206}Pb$ in zircon. This systematic inaccuracy can reach a maximum magnitude of 107 ky too young for the extreme case of no initial $^{230}Th$ present in the zircon, regardless of the zircon age. However, the exact magnitude of this correction is difficult to quantify without knowledge of the Th/U ratio of the magma from which the zircon has crystallized. The latter ratio is commonly estimated by measuring the Th/U ratio of the whole rock, glass (e.g., pumice) and/or melt inclusions. Tuffs in the Green River Formation are extensively altered and their original composition is unknown. Petrographic analysis of these tuffs has shown that they contain primary quartz, sanidine, biotite and hornblende phenocrysts, and they have been interpreted to range in composition from andesitic to rhyodacitic (Bradley, 1964; Iijima and Hay, 1968). We rely on direct measurement of melt inclusions within quartz from the Bishop Tuff ($2.81 \pm 0.32$; Crowley et al., 2007), which is consistent with a survey of Th/U from felsic tuffs measured with neutron activation from EarthChem database ($3.4 \pm 1.2$, $N = 432$; www.earthchem.org). Because there is good overlap between the empirical value and the direct measurement, we use the value of $2.8 \pm 1$ ($2\sigma$) as the best estimate for the Th/U ratio in the parent magma. Relying on this assumed Th/U results in Th corrections ranging from 83 ky to 98 ky applied to our single zircon analyses and with associated uncertainties incorporated in the reported date uncertainties. The value of 2.8 is also consistent with reported Th/U values for rocks of the Absaroka volcanic province with a similar age range (Hiza, 1999) that are a likely source for the ashes of the Green River Formation.

The assumed magma Th/U ratio of $2.8 \pm 1$ covers the lower range of possible values for common magma compositions, but Th/U ratios of up to 6 are not inconceivable for felsic magmas. However, the magnitude of Th correction decreases exponentially at higher magma Th/U ratios, such that between assumed ratios of 4 and 6, the correction corresponding to our analyses drops below 8 ky (see Supplementary Materials, Fig. S4). In conclusion, assuming extreme magma Th/U outside the range used in our Th corrections will not affect the accuracy of our age results by more than 8 ky beyond the reported uncertainties.

### 5.3. Comparison to previous geochronology

Previously reported $^{40}Ar/^{39}Ar$ and U–Pb dates (Smith et al., 2003, 2006, 2008, 2010) are based on analyses of multi-crystal aliquots. Grouping crystals together assumes that the crystals are from a single population, but if there is evidence for presence of older crystals it will bias the weighted mean age toward an older value, even if obvious outliers are removed from the age population of multi-crystal dates. For example, the $^{40}Ar/^{39}Ar$ weighted mean age of the Layered tuff ($50.11 \pm 0.09$; Smith et al., 2006, 2010) is based on analyses of 10- and 20-crystal populations of sanidine per aliquot, yet it is still necessary to exclude 8 dates that are up to 6 million years older than the calculated weighted mean. Considering the large number of crystals per aliquot, the original range of old outlier ages must be even larger. The previously inferred age of the Layered tuff is a maximum estimate for these reasons, and we cannot rule out the existence of older crystals that were similarly entrained during eruption in other ashes and not statistically eliminated due to the multi-crystal aliquots.

In addition to the potential bias of multi-crystal dates towards old values, there is a potential bias of sanidine-based dates towards young values. Smith et al. (2003) took an innovative approach that allowed dating of unaltered sanidine using air abrasion to remove an authigenic rim surrounding an un-altered core. However, there is no way to guarantee full removal of the younger authigenic growth from all crystals, especially within cracks in the crystals. Therefore there is a potential bias for ashes dated by sanidines to be too young, especially for older ashes that were deposited in a lake that was more frequently hypersaline (thickest and most evaporate-rich beds are in the lower part of the Wilkins Peak Member; Culbertson et al., 1980). We conclude that whether all/some of the ages reported here overlap with previous ages or not, the two geochronologies are not comparable, and it is not the purpose of this paper to evaluate systematic biases in the Ar–Ar system.

Another important difference between the two methods is the analytical uncertainty associated with an individual analysis. Ultimately, the individual uncertainties determine the resolution possible for testing astronomical calibrations. The analytical uncertainties ($2\sigma$) for zircon dates from outcrop samples are less than 70 ky for over half of the zircons and less than 150 ky for most, whereas the analytical uncertainties ($2\sigma$) associated with single $^{40}Ar/^{39}Ar$ analyses (of multiple crystals) are no less than 150 ky and are mostly much larger, and uncertainties for the previously published multi-crystal analyses included in the U–Pb date (Firehole tuff) are at least 60 ky and mostly much larger as well (Smith et al., 2010). The weighted mean dates reported in previous studies are therefore much less precise ($2\sigma$ analytical uncertainties of 90–210 ky for $^{40}Ar/^{39}Ar$ ages and 190 ky for the Firehole tuff U–Pb age) compared to the uncertainties reported here for the five ashes dated in both studies (12–40 ky; Fig. 2, Table 1).

Overall, the shape of the new age-depth curve for the Wilkins Peak Member is significantly different from the curve generated by the previous geochronology and the new ages imply a lower sediment accumulation rate and thus greater age range for the Wilkins Peak Member (Figs. 2, 3).

## 6. Re-evaluation of the orbital forcing hypothesis

### 6.1. Re-testing orbital age models

The new geochronology forces rejection of the previously accepted age models (Section 4.4), except for the 125 ky model (Fig. 3). The 125 ky model (Machlus et al., 2008; Fig. 3; Section 4.2) cannot be falsified with the high precision U–Pb ages in this study because the model includes large uncertainties that overlap with the new ages. Acceptance of this model would imply a longer duration for the main period of short-eccentricity at about 50 Ma. Overall there are two pairs of main eccentricity periods: ~95 ky and ~99 ky, and ~124 ky and ~131 ky (calculated by Berger and Loutre, 1991 for the last 10 m.y. and Laskar et al., 2011a, 2011b for the last 50 m.y.). The latter pair with a mean period close to 125 ky is the less dominant pair for the last 50 m.y. (Laskar et al., 2011a) but the calculation of orbital parameters is less precise beyond 50 Ma (Laskar et al., 2011a, 2011b; Westerhold et al., 2012) and therefore the overlap of the 125 ky age model with the U–Pb ages might be attributable to a longer mean eccentricity period. Although we do not reject this possibility, and we recognize that if it could be demonstrated it would be important, the age constraints are not yet strong enough to make the case for a longer mean eccentricity period. In the following we explore an alternative, that is distortion of the record from variable sediment accumulation rate as a possible explanation for this apparently longer eccentricity period.

### 6.2. Iterative procedure to identify the orbital signal in cyclic strata

In the ideal case, when numerous datable ashes area available, a detailed chronostratigraphy can be utilized to identify an existing orbital signal that may be distorted by sedimentary processes. Such ideal geochronology would need to include at least one age per hypothesized cycle, each with an uncertainty that is smaller than half the period of the tested cycle. Such a requirement guarantees no *a-priori* assumptions about sediment accumulation rates (i.e. no orbital tuning is required) and therefore allows identifying the orbital signal and potential distortions. As the current geochronology fulfills only part of this requirement, an intermediate testing step is proposed that allows the identification of significant gaps or other disruptions to sediment accumulation rate, that may distort an orbitally-paced sedimentary signal.

The intermediate testing step is set up by superimposing two alternative age-depth models (thick and dotted lines in Fig. 5) on the simple linear age-depth model connecting the U–Pb ages (diamonds in Fig. 5). These two models honor the existing geochronology, i.e., they pass through all the U–Pb ages within their stated uncertainties, but diverge from the sediment accumulation rates of the simple age model connecting the ages (cf. two plotted lines and the imaginary lines connecting the U–Pb ages in Fig. 5). An age difference between one of the two age models and the line connecting the U–Pb ages defines a priority interval for further radioisotopic testing. Any interval in which this difference is larger than the radioisotopic uncertainty of ~20 ky is a candidate for further dating (e.g., see arrows in Fig. 5). New high-resolution age(s) for the testing interval(s) will then direct the next adjustment to the alternative age models and the next iteration of this intermediate step. There are abundant volcanic ashes throughout all of these intervals (e.g., Culbertson et al., 1980), and abundant marker beds facilitate correlation of additional ashes to selected cores in the basin center (see Section 2.3 for marker beds), so several more iterations are likely to be practical and can continue until there is enough age control to construct a more complete test of the astronomical calibration for the Wilkins Peak Member.

### 6.3. Implications for cyclic records and solution for orbital parameters

An astronomical calibration of the Wilkins Peak Member may suggest modified periods for orbital parameters, compared to those known for the Neogene, especially for the time interval prior to about 50 Ma. At that interval, the validity of the orbital solution is difficult to assess (see the Westerhold et al., 2012; comparison of the two latest orbital solutions: LA2010 and LA2011 of Laskar et

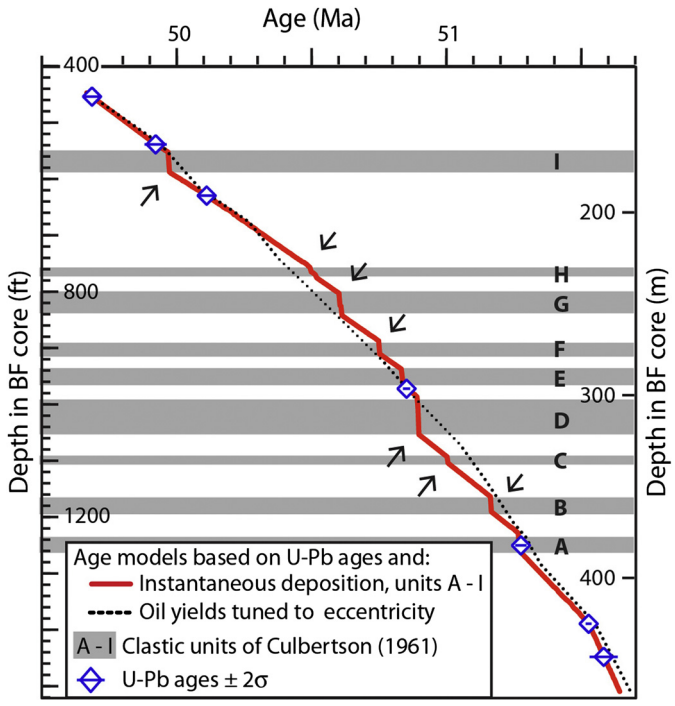


**Fig. 5.** Alternative *ad-hoc* age models that coincide with the reported U–Pb ages but mostly diverge from each other: (1) an extreme "fast" model (thick line) assumes instant deposition for clastic units A through I of Culbertson (1961; grey horizontal bars) and for trona beds (too thin to be distinguished at this scale), whereas intervening rates between these beds vary as needed to honor the age constraints; (2) an orbital age model (dotted line) created by tuning the Fischer assay record of core BF (Roehler, 1991a) to the nominal solution for eccentricity parameter (LA2010a) of Laskar et al. (2011a) using AnalySeries (Paillard et al., 1996). The orbital model includes intervals with both "slow" and "fast" apparent accumulation rates compared with the first model. Arrows mark depths where these age models can be distinguished from one another by additional U–Pb ages with similar precision as reported here. The details of constructing the orbital age model are provided in Supplementary Material Fig. S5. Tuff names from top to bottom: Sixth tuff; Layered tuff; Main tuff; Grey tuff; Second tuff; Firehole tuff; and 1448 tuff.

al., 2011a, 2011b respectively), but the modulation of short eccentricity between 50 Ma and 54 Ma is similar in the orbital solution LA2010d and the more precise solution LA2011 (Westerhold et al., 2012). Radioisotopic dating as reported here can facilitate the validation of different orbital solutions at the time interval between 50 Ma and 54 Ma. The additional solutions (LA10b, LA10c, LA10d of LA2010; Laskar et al., 2011a) differ from the nominal solution (LA10a of Laskar et al., 2011a) that was used in this example as the target curve for tuning (see details in Supplementary Material Fig. S5), and hence demonstrate an opportunity to calibrate the orbital solution itself from the record of the Green River Formation with future detailed dating.

The strategy applied here to testing the cyclicity in the Wilkins Peak Member is suitable for testing any cyclic record and for establishing a more rigorous, iterative approach for astronomical calibration of the geological timescale. In cases where sparse volcanic ashes are intercalated with cyclic strata the issue of testing can be tackled in several ways. One option is to date thin ash laminae that were not datable before and can be dated now at relatively high precision, as demonstrated by the reported data for the 1448 tuff. Another option is a combination of radioisotopic data of the precision presented here with methods of time series analysis intended for locating gaps (e.g., Evolutive Harmonic Analysis, Meyers et al., 2001; also see Herbert, 1994; Weedon, 2003) and with evolutive statistical methods that can quantitatively assess the potential age-depth models that agree with orbital forcing of the strata in question (e.g., evolutive Average Spectral Misfit: Meyers et al., 2012; and application of the Bayesian inverse method of Malinverno et al., 2010 for selected intervals).

## 7. Conclusions

The new high precision U–Pb zircon depositional ages from the seven ash beds within the Wilkins Peak Member of the Green River Formation are consistent with the 125 ky model of Machlus et al. (2008) but inconsistent with all of the other published orbital age models (Fig. 3). Our new data suggest either that the mean eccentricity period during the early–middle Eocene was 125 ky or argue for alternative age-depth models that include a combination of periodic and non-periodic sediment accumulation. We use a new iterative approach to identify how targeted future high-resolution U–Pb dating can test the remaining alternative age models. Beyond the specific conclusions about the cyclicity of the Wilkins Peak Member, two other general conclusions can be drawn from this work: (1) The current state-of-the-art in high precision CA-TIMS U–Pb geochronology of single zircon crystals provides the opportunity to test tuning of Early Cenozoic cyclic records at $2\sigma$ precision comparable to a single precession period; (2) U–Pb zircon dates can be obtained from small core samples, thus greatly expanding the possible application of this strategy to both marine and terrestrial records.

## Acknowledgements

We would like to thank the personnel of the USGS Core Research Center and John Dyni for their help in viewing and sampling cores, and Donald and Ernestine Gamble for their help in sampling outcrops in Firehole Canyon. We also thank the editor Gideon Henderson and our reviewers, Stephen Meyers and an anonymous reviewer, for their detailed comments, which improved the manuscript significantly. This research was supported by National Science Foundation grants EAR 0720086 (to Hemming and Machlus) and 0720253 (to Bowring) and by the Lamont Climate Center. Lamont-Doherty Earth Observatory contribution 7848.

## Appendix A. Supplementary material

Supplementary material related to this article can be found online at http://dx.doi.org/10.1016/j.epsl.2014.12.009.

## References

Aswasereelert, W., Meyers, S.R., Carroll, A.R., Peters, S.E., Smith, M.E., Feigl, K.L., 2013. Basin-scale cyclostratigraphy of the Green River Formation, Wyoming. Geol. Soc. Am. Bull. 125, 216–228.

Bereskin, S.R., Morgan, C.D., 2001. Fluvial-lacustrine oil reservoirs in the middle member of the Eocene Green River Formation, south-central Uinta Basin, Utah. In: AAPG Annual Meeting, 2001, Am. Assoc. Pet. Geol. Bull. 85. Supplement.

Berger, A., Loutre, M., 1991. Insolation values for the climate of the last 10 million years. Quat. Sci. Rev. 10, 297–317.

Berger, A., Loutre, M.F., Laskar, J., 1992. Stability of the astronomical frequencies over the Earth's history for paleoclimate studies. Science 255, 560–566.

Bowring, S.A., Schoene, B., Crowley, J.L., Ramezani, J., Condon, D.J., 2006. High-precision U–Pb zircon geochronology and the stratigraphic record: progress and promise. In: Olszewski, T.D. (Ed.), Geochronology: Emerging Opportunities. In: Paleontol. Soc. Pap., vol. 12, pp. 25–45.

Bowring, J.F., McLean, N.M., Bowring, S.A., 2011. Engineering cyber infrastructure for U–Pb geochronology: Tripoli and U–Pb_Redux. Geochem. Geophys. Geosyst. 12, Q0AA19.

Bradley, W.H., 1929. The varves and climate of the Green River epoch. U.S. Geological Survey Professional Paper 158, pp. 87–110.

Bradley, W.H., 1964. Geology of Green River Formation and associated Eocene rocks in southwestern Wyoming and adjacent parts of Colorado and Utah. U.S. Geological Survey Professional Paper 496-A, pp. A1–A86.

Brownfield, M.E., Self, J.G., Mercier, T.J., 2011. Fischer assay histograms of oil-shale drill cores and rotary cuttings from the Great Divide, Green River, and Washakie

Basins, Southwestern Wyoming. In: U.S. Geological Survey Oil Shale Assessment Team (Ed.), Oil Shale Resources of the Eocene Green River Formation, Greater Green River Basin, Wyoming, Colorado, and Utah. In: U.S. Geol. Surv. Digit. Data Ser., vol. DDS-69-DD. Chapter 6, 6 pp.
Burgess, S.D., Bowring, S., Shen, S.Z., 2014. High-precision timeline for Earth's most severe extinction. Proc. Natl. Acad. Sci. USA 111, 3316–3321.
Crowley, J.L., Schoene, B., Bowring, S.A., 2007. U–Pb dating of zircon in the Bishop Tuff at the millennial scale. Geology 35, 1123.
Culbertson, W.C., 1961. Stratigraphy of the Wilkins Peak member of the Green River Formation, Firehole Basin Quadrangle, Wyoming, Article 348. U.S. Geological Survey Professional Paper 424-D, pp. 170–173.
Culbertson, W.C., 1966. Trona in the Wilkins Peak Member of the Green River Formation, southwestern Wyoming. U.S. Geological Survey Professional Paper 550B, pp. B159–B164.
Culbertson, W.C., Smith, J.W., Trudell, L.G., 1980. Oil shale resources and geology of the Green River Formation in the Green River Basin, Wyoming. Laramie Energy Technology Center LETC/RI-80/6. 102 pp.
Dickinson, W.R., Klute, M.A., Hayes, M.J., Janecke, S.U., Lundin, E.R., McKittrick, M.A., Olivares, M.D., 1988. Paleogeographic and paleotectonic setting of Laramide sedimentary basins in the central Rocky Mountain region. Geol. Soc. Am. Bull. 100, 1023–1039.
Eugster, H.P., Hardie, L.A., 1975. Sedimentation in an ancient playa-lake complex; the Wilkins Peak Member of the Green River Formation of Wyoming. Geol. Soc. Am. Bull. 86, 319–334.
Fischer, A.G., Roberts, L.T., 1991. Cyclicity in the Green River Formation (lacustrine Eocene) of Wyoming. J. Sediment. Petrol. 61, 1146–1154.
Gradstein, F.M., Ogg, J.G., Schmitz, M.D., Ogg, G.M., 2012. The Geologic Time Scale 2012. Elsevier, Amsterdam. 1144 pp.
Grande, L., 1984. Paleontology of the Green River Formation, with a review of the fish fauna. Bull.- Geol. Surv. Wyo. 63, 333 pp.
Hayden, F.V., 1869. Preliminary field report of the United States Geological Survey of Colorado and New Mexico. Government Printing Office, Washington. 155 pp.
Herbert, T.D., 1994. Reading orbital signals distorted by sedimentation; models and examples. In: de Boer, P.L., Smith, D.G. (Eds.), Orbital Forcing and Cyclic Sequences. In: Spec. Publ. Int. Assoc. Sedimentol., vol. 19, pp. 483–507.
Hinnov, L.A., Hilgen, F., 2012. Cyclostratigraphy and astrochronology. In: Gradstein, F.M., Ogg, J.G., Schmitz, M.D., Ogg, G.M. (Eds.), A Geologic Time Scale 2012. Elsevier, Amsterdam, pp. 63–83.
Hinnov, L.A., 2013. Cyclostratigraphy and its revolutionizing applications in the earth and planetary sciences. Geol. Soc. Am. Bull. 125, 1703–1734.
Hiza, M.M., 1999. The geochemistry and geochronology of the Eocene Absaroka volcanic province, northern Wyoming and Southwest Montana, USA. Doctoral thesis. 243 pp.
Iijima, A., Hay, R.L., 1968. Analcime composition in tuffs of the Green River Formation of Wyoming. Am. Mineral. 53, 184–200.
Kuiper, K.F., Deino, A., Hilgen, F.J., Krijgsman, W., Renne, P.R., Wijbrans, J.R., 2008. Synchronizing rock clocks of Earth history. Science 320, 500–504.
Laskar, J., Robutel, P., Joutel, F., Gastineau, M., Correia, A.C.M., Levrard, B., 2004. A long-term numerical solution for the insolation quantities of the Earth. Astron. Astrophys. 428, 261–285.
Laskar, J., Fienga, A., Gastineau, M., Manche, H., 2011a. La2010: a new orbital solution for the long-term motion of the Earth. Astron. Astrophys. 532, A89.
Laskar, J., Gastineau, M., Delisle, J.B., Farrés, A., Fienga, A., 2011b. Strong chaos induced by close encounters with Ceres and Vesta. Astron. Astrophys. 532, L4.
Love, J.D., 1964. Uraniferous phosphatic lake beds of Eocene age in Intermontane basins of Wyoming and Utah. U.S. Geological Survey Professional Paper 474-E, E1-E66.
Machlus, M.L., Olsen, P.E., Christie-Blick, N., Hemming, S.R., 2008. Spectral analysis of the lower Eocene Wilkins Peak Member, Green River Formation, Wyoming; support for Milankovitch cyclicity. Earth Planet. Sci. Lett. 268, 64–75.
Malinverno, A., Erba, E., Herbert, T.D., 2010. Orbital tuning as an inverse problem: chronology of the early Aptian oceanic anoxic event 1a (Selli Level) in the Cismon APTICORE. Paleoceanography 25, PA2203.
Mattinson, J.M., 2005. Zircon U–Pb chemical abrasion ("CA-TIMS") method: combined annealing and multi-step partial dissolution analysis for improved precision and accuracy of zircon ages. Chem. Geol. 220, 47–66.
McLean, N.M., Bowring, J.F., Bowring, S.A., 2011. An algorithm for U–Pb isotope dilution data reduction and uncertainty propagation. Geochem. Geophys. Geosyst. 12, Q0AA18.
Meyers, S.R., 2008. Resolving Milankovitchian controversies; the Triassic Latemar Limestone and the Eocene Green River Formation. Geology 36, 319–322.
Meyers, S.R., Sageman, B.B., Hinnov, L.A., 2001. Integrated quantitative stratigraphy of the Cenomanian–Turonian Bridge Creek Limestone Member using evolutive harmonic analysis and stratigraphic modeling. J. Sediment. Res. 71, 628–644.
Meyers, S.R., Sageman, B.B., 2007. Quantification of deep-time orbital forcing by average spectral misfit. Am. J. Sci. 307, 773–792.
Meyers, S.R., Sageman, B.B., Arthur, M.A., 2012. Obliquity forcing of organic matter accumulation during Oceanic Anoxic Event 2. Paleoceanography 27, PA3212.
Paillard, D., Labeyrie, L., Yiou, P., 1996. Macintosh program performs time-series analysis. EOS Trans. AGU 77, 379.
Pietras, J.T., Carroll, A.R., Singer, B.S., Smith, M.E., 2003. 10 k.y. depositional cyclicity in the early Eocene: stratigraphic and $^{40}Ar/^{39}Ar$ evidence from the lacustrine Green River Formation. Geology 31, 593–596.
Pietras, J.T., Carroll, A.R., 2006. High-resolution stratigraphy of an underfilled lake basin: Wilkins Peak Member, Eocene Green River Formation, Wyoming, U.S.A. J. Sediment. Res. 76, 1197–1214.
Prothero, D.R., 1996. Magnetic stratigraphy and biostratigraphy of the middle Eocene Uinta Formation, Uinta Basin, Utah. In: Prothero, D.R., Emry, R.J. (Eds.), The Terrestrial Eocene–Oligocene Transition in North America. Cambridge University Press, New York, United States, pp. 3–24.
Ramezani, J., Hoke, G.D., Fastovsky, D.E., Bowring, S.A., Therrien, F., Dworkin, S.I., Atchley, S.C., Nordt, L.C., 2011. High-precision U–Pb zircon geochronology of the Late Triassic Chinle Formation, Petrified Forest National Park (Arizona, USA); temporal constraints on the early evolution of dinosaurs. Geol. Soc. Am. Bull. 123, 2142–2159.
Renne, P.R., Swisher, C.C., Deino, A.L., Karner, D.B., Owens, T.L., DePaolo, D.J., 1998. Intercalibration of standards, absolute ages and uncertainties in $^{40}Ar/^{39}Ar$ dating. Chem. Geol. 145, 117–152.
Rivera, T.A., Storey, M., Schmitz, M.D., Crowley, J.L., 2013. Age intercalibration of $^{40}Ar/^{39}Ar$ sanidine and chemically distinct U/Pb zircon populations from the Alder Creek Rhyolite Quaternary geochronology standard. Chem. Geol. 345, 87–98.
Roehler, H.W., 1991a. Identification of oil shale and trona beds and their geophysical log responses in the Energy Research and Development Administration Blacks Fork No. 1 corehole, Eocene Green River Formation, southwest Wyoming. U.S. Geological Survey Miscellaneous Field Studies Map MF-2158, 1 sheet.
Roehler, H.W., 1991b. Correlation and depositional analysis of oil shale and associated rocks in the Eocene Green River Formation, Greater Green River Basin, southwest Wyoming. U.S. Geological Survey Miscellaneous Investigations Series I-2226. 2 sheets.
Roehler, H.W., 1992a. Correlation, composition, areal distribution, and thickness of Eocene stratigraphic units, Greater Green River Basin, Wyoming, Utah, and Colorado. U.S. Geological Survey Professional Paper 1506-E, pp. E1–E49.
Roehler, H.W., 1992b. Description and correlation of Eocene rocks in stratigraphic reference sections for the Green River and Washakie basins, southwest Wyoming. U.S. Geological Survey Professional Paper 1506-D, pp. D1–D83.
Roehler, H.W., 1993. Eocene climates, depositional environments, and geography, Greater Green River Basin, Wyoming, Utah, and Colorado. U.S. Geological Survey Professional Paper 1506-F, pp. F1–F74.
Smith, M.E., 2007. The stratigraphy and geochronology of the Green River Formation, western United States. Unpublished PhD thesis, University of Wisconsin-Madison, 318 pp.
Smith, M.E., Singer, B., Carroll, A.R., 2003. $^{40}Ar/^{39}Ar$ geochronology of the Eocene Green River Formation, Wyoming. Geol. Soc. Am. Bull. 115, 549–565.
Smith, M.E., Singer, B.S., Carroll, A.R., Fournelle, J.H., 2006. High-resolution calibration of Eocene strata; $^{40}Ar/^{39}Ar$ geochronology of biotite in the Green River Formation. Geology 34, 393–396.
Smith, M.E., Carroll, A.R., Singer, B.S., 2008. Synoptic reconstruction of a major ancient lake system; Eocene Green River Formation, western United States. Geol. Soc. Am. Bull. 120, 54–84.
Smith, M.E., Chamberlain, K.R., Singer, B.S., Carroll, A.R., 2010. Eocene clocks agree; coeval $^{40}Ar/^{39}Ar$, U–Pb, and astronomical ages from the Green River Formation. Geology 38, 527–530.
Smoot, J.P., 1983. Depositional subenvironments in an arid closed basin; the Wilkins Peak Member of the Green River Formation (Eocene), Wyoming, USA. Sedimentology 30, 801–827.
Tsukui, K., Clyde, W.C., 2012. Fine-tuning the calibration of the early to middle Eocene geomagnetic polarity time scale: paleomagnetism of radioisotopically dated tuffs from Laramide foreland basins. Geol. Soc. Am. Bull. 124, 870–885.
Weedon, G.P., 2003. Time-Series Analysis and Cyclostratigraphy: Examining Stratigraphic Records and Environmental Cycles. Cambridge University Press, Cambridge, UK. 276 p.
Westerhold, T., Röhl, U., Laskar, J., 2012. Time scale controversy: accurate calibration of the early Paleogene. Geochem. Geophys. Geosyst. 13, Q06015.
Wotzlaw, J.-F., Schaltegger, U., Frick, D.A., Dungan, M.A., Gerdes, A., Günther, D., 2013. Tracking the evolution of large-volume silicic magma reservoirs from assembly to supereruption. Geology 41, 867–870.
Wotzlaw, J.F., Guex, J., Bartolini, A., Gallet, Y., Krystyn, L., McRoberts, C.A., Taylor, D., Schoene, B., Schaltegger, U., 2014. Towards accurate numerical calibration of the Late Triassic: high-precision U–Pb geochronology constraints on the duration of the Rhaetian. Geology 42, 571–574.